ROYAL SOCIETY OF CHEMISTRY

EDGE ARTICLE

Check for updates

Droplet-mediated kinetic-to-thermodynamic transition for the fabrication of uniform 1D and 2D nanostructures from conjugated homopolymers

Zehua Li, [ID] Yufan Gu, Yiheng Liu, Siyu Ji and Xu-Hui Jin [ID] *

Kinetically controlled nonequilibrium self-assembly is ubiquitous in biological systems and plays a critical role in self-organization. Yet, achieving precise control over such nonequilibrium phase transitions remains a fundamental challenge in materials design. Here, we demonstrate that conjugated homopolymers can form uniform nanostructures with well-defined dimensions through a solution-phase kinetic-to-thermodynamic transition (KTT). This process proceeds *via* a rationally designed liquid-like intermediate that mediates nucleation and directional growth, affording morphologically pure nanostructures. Remarkably, the solvent environment critically dictates nucleation within the liquid-like intermediates, enabling the formation of either one-dimensional (1D) nanowires or two-dimensional (2D) nanoplatelets from the same polymer. Seed-assisted KTT further reveals that the liquid-like intermediate imparts both morphologies with living growth behavior, yielding nanostructures with precisely tunable dimensions across multiple length scales. These findings provide key insights into programmable kinetically controlled nonequilibrium self-assembly of π-conjugated polymers and establish a versatile strategy for fabricating structurally defined nanomaterials.

Introduction

The self-assembly of polymeric materials into nanostructures with well-defined morphologies has attracted widespread attention due to their potential in diverse applications, from electronics to biomedicine.[1–5] Precise control over both shape and size is particularly critical, as these parameters strongly influence key functional properties. For instance, nanoscale dimensions can profoundly affect exciton transport,[6,7] charge-carrier mobility,[8–10] and photocatalytic efficiency[11] in optoelectronic and energy-conversion systems, while also modulating interfacial interactions and mechanical robustness in biomedical and structural materials.[12–16] However, achieving such control remains a significant challenge, owing to the complex interplay between kinetic and thermodynamic factors that govern the assembly process.[3,17] This has driven increasing efforts to devise new strategies capable of producing polymer nanostructures with tunable dimensions and high structural fidelity.
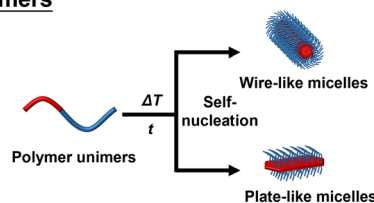
Living crystallization-driven self-assembly (CDSA) has emerged as a powerful strategy for the controlled fabrication of nanoscale polymeric materials and has been widely applied to the construction of one-dimensional (1D) and two-dimensional (2D) nanostructures from block copolymers.[3,4,18–20] In typical CDSA processes, polymers are fully dissolved in solution as

unimers[21,22] and, in the presence of seeds, undergo seeded growth on pre-existing crystalline surfaces. This kinetically guided attachment, where polymer chains add to seeds faster than self-nucleation, yields nanostructures with predictable morphologies and dimensions that scale linearly with the unimer-to-seed ratio.[6,23–28] Recent studies have further demonstrated *in situ* crystallization-driven nanoparticlization, producing length-tunable 1D conjugated polymer nanoparticles during living Suzuki–Miyaura polymerization.[29] Nevertheless, polymers are also known to form kinetically trapped, metastable assemblies,[17,30,31] which can undergo structural reorganization into more thermodynamically favored forms.[32,33] Such kinetically favored metastable assembly to thermodynamically favored form transition,[34] abbreviated as "kinetic-to-thermodynamic transition" (KTT), is ubiquitous in biological systems and has been shown to yield assembly outcomes distinct from those generated under purely thermodynamic control.[34–37] For example, in supramolecular polymer systems, morphologies or chiralities arising from KTT can differ significantly from those formed *via* equilibrium pathways.[34] Despite their prevalence and functional significance,[38,39] these nonequilibrium assembly pathways have been rarely explored in the context of living polymer self-assembly. Integrating kinetic phase transitions into CDSA, therefore, holds great potential for expanding the structural complexity and functional versatility of polymer nanomaterials beyond conventional thermodynamic limits.

School of Chemistry and Chemical Engineering, Beijing Institute of Technology, Beijing, 102488, China. E-mail: xuhui.jin@bit.edu.cn
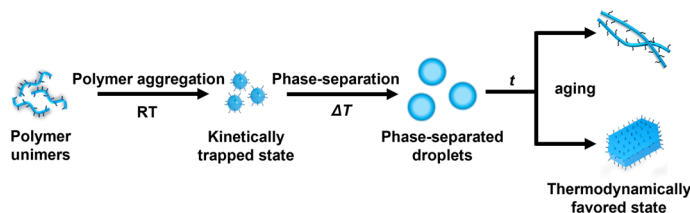
Classical Work: Self-Assembly of Conjugated Block Copolymers

➤ Fully dissolved block copolymers assemble into 1D cylindrical and 2D lamellar micelles via thermodynamically driven processes.

This Work: Droplet-Mediated Kinetic-to-Thermodynamic Transition of Conjugated Homopolymers

✓ Kinetically trapped nanoparticles of conjugated homopolymers undergo transformation through flowable droplet intermediates, yielding thermodynamically stable one-dimensional (1D) nanowires or two-dimensional (2D) nanoplatelets.

Scheme 1 Schematic representation of the proposed strategy utilizing droplets derived from the phase separation of metastable kinetically trapped assemblies for a controlled self-assembly process.

Homopolymers are among the most common macromolecular materials. Compared with block copolymers, they have been more extensively studied and applied. However, their lack of solvophilic segments often leads to poor colloidal stability, rapid aggregation, and the formation of metastable structures that are difficult to control. These intrinsic limitations have long hindered the precise fabrication of homopolymer-based nanostructures. Previous work addressed this challenge through a seed-guided living CDSA process, where conjugated polyenyne homopolymers with enhanced solubility from cascade metathesis and metallotropy polymerization assembled into size-tunable 2D nanorectangles (0.1–3.0 μm^2) via biaxial growth.[40] Herein, we present a novel nonequilibrium strategy to program the solution self-assembly of conjugated homopolymers (Scheme 1), a class of π-conjugated materials widely used in optoelectronic devices. We demonstrate that introducing stable, liquid-like intermediate states during the KTT of conjugated homopolymers enables the formation of nanostructures with well-defined morphologies. We systematically investigated the conditions governing the emergence of these intermediates and examined their impact on the final assembly. Notably, the solvent environment was found to direct polymer nucleation within these liquid-like intermediates, allowing the same polymer system to yield either one-dimensional (1D) nanowires or two-dimensional (2D) nanoplatelets. Furthermore, the presence of liquid-like intermediates facilitates seed-assisted KTT, affording precise control over both morphology and size. This strategy expands the toolkit for conjugated polymer assembly and provides a versatile, accessible approach to tailoring nanoscale architectures via nonequilibrium pathways.

Results and discussion

Non-equilibrium assembly and solvent-directed morphological transformation

We initially checked the kinetically controlled nonequilibrium self-assembly of conjugated homopolymers, poly[3-(2-(2-(2-methoxyethoxy)ethoxy)ethoxy)methylthiophene] (P(T-PEG$_3$)$_{25}$, $M_n = 6.53$ kg mol^{-1}, $Đ_M = 1.60$) in solution. Polythiophene (PT) was selected as a model polymer due to its extensive prior study and well-characterized properties. Polyethylene glycol (PEG) was introduced as a polar side chain to enhance the hydrophilicity of the hydrophobic conjugated backbone, promoting the formation of liquid-like intermediates during the phase transition process (detailed characterizations are provided in Fig. S1–S3 and Table S1).[41,42] Kinetically trapped assemblies (KTAs) of P(T-PEG$_3$)$_{25}$ homopolymers were fabricated via a rapid one-pot solvent-precipitation method. Polar solvents such as water or ethanol were chosen as poor solvents to induce self-assembly. Due to the hydrophobic nature of the polythiophene backbone, rapid aggregation occurred upon exposure to these polar media. Meanwhile, the PEG$_3$ side chains, which are soluble in both water and ethanol, imparted excellent colloidal stability to the resulting aggregates. Specifically, a THF solution of P(T-PEG$_3$)$_{25}$ (20 μL, 10 mg mL^{-1}) was added dropwise into either 400 μL of water or 1 mL of ethanol at room temperature (RT). After aging for 12 h, both THF/EtOH and THF/H$_2$O mixtures displayed a noticeable color change from light yellow to orange, accompanied by red-shifted absorption (Fig. 1b and c), indicating the formation of polymer aggregates. The resulting polymer aggregates were characterized by transmission electron microscopy (TEM) and dynamic light scattering (DLS). TEM images confirmed the formation of KTAs, with average diameters of ca. 46 nm in the THF/EtOH mixture (1 : 50, v/v, 0.2 mg mL^{-1}) and ca. 52 nm in the THF/H$_2$O mixture (1 : 20, v/v, 0.5 mg mL^{-1}) (Fig. 1d, e, and Table S2).

Upon in situ thermal treatment, these KTAs underwent a kinetic-to-thermodynamic morphological transition (Fig. 1a). In the absence of heating, KTAs in THF/EtOH (1 : 50, v/v) or THF/H$_2$O (1 : 20, v/v) solutions retained their initial morphology for at least one week (Fig. S4a and b). However, as shown in Fig. 1f, heating the THF/EtOH solution at 60 °C for 12 hours, followed by aging at RT for 2 days, led to the complete
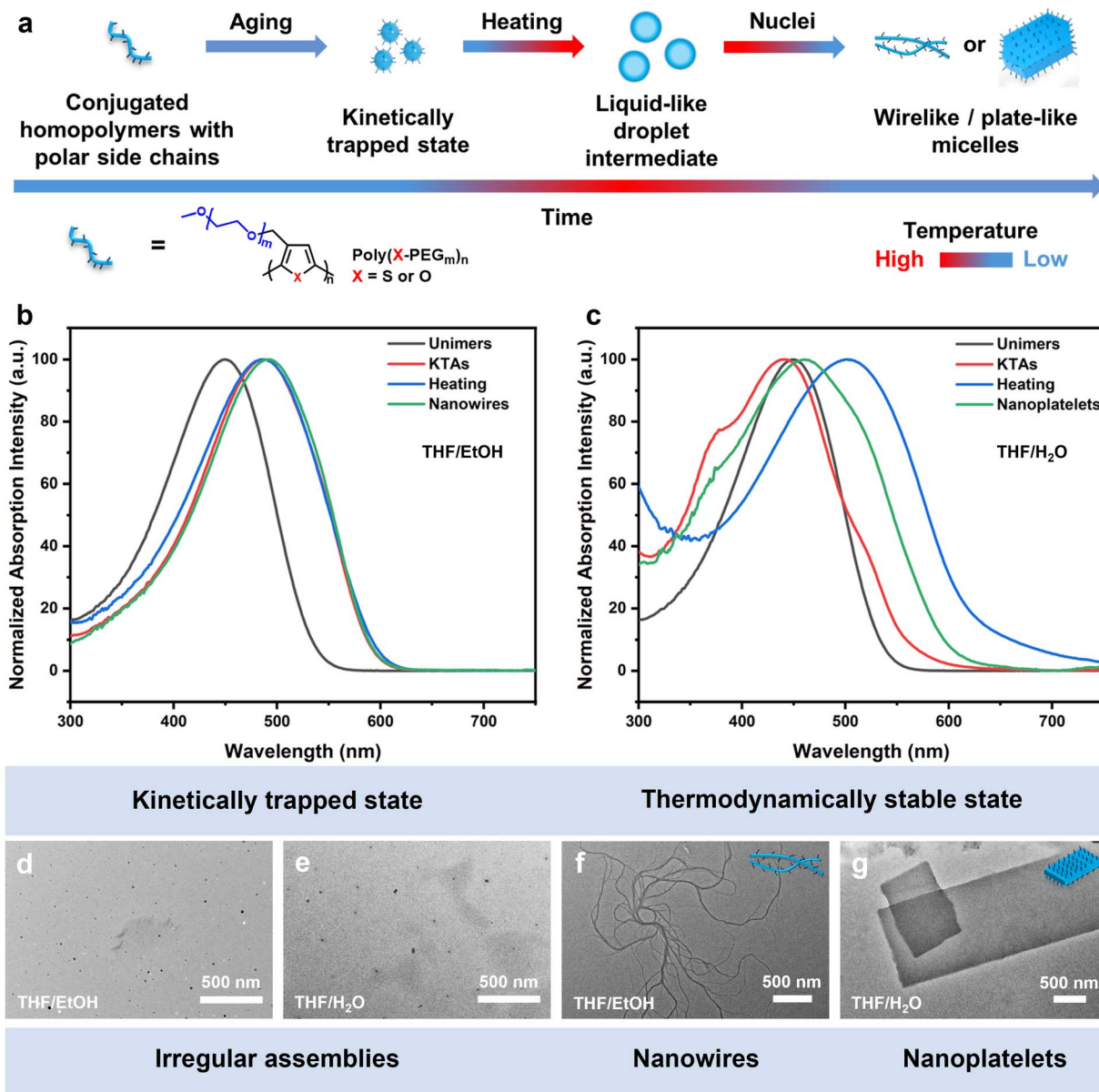
Fig. 1 Characterization of thiophene–based nanoparticles of different morphologies. (a) Schematic illustration of different morphologies in the self-assembly of P(T-PEG$_3$)$_{25}$ homopolymers. Normalized absorption of P(T-PEG$_3$)$_{25}$ in the (b) THF/EtOH solution and (c) THF/H$_2$O solution. Representative TEM micrographs of (d) P(T-PEG$_3$)$_{25}$ KTAs in the THF/EtOH solution, (e) P(T-PEG$_3$)$_{25}$ KTAs in the THF/H$_2$O solution, (f) P(T-PEG$_3$)$_{25}$ nanowires, and (g) P(T-PEG$_3$)$_{25}$ nanoplatelets. Scale bar = 500 nm for (a–e).

disappearance of the initial nanoparticles and the formation of 1D wire-like structures. Interestingly, the same thermal treatment in the THF/H$_2$O system yielded 2D plate-like structures with well-defined rectangular geometries, as confirmed by TEM (Fig. 1g). UV-vis absorption spectra revealed broad, featureless profiles (λ = 1.96–4.09 eV) for the 1D nanowires, whereas the 2D platelets exhibited well-resolved vibronic structures (λ = 1.89–2.54 eV), suggesting a higher degree of molecular ordering. These findings collectively underscore the critical role of solvent environment in directing both the morphology and internal ordering of P(T-PEG$_3$)$_{25}$ during the KTT process.

Role of liquid-like intermediates in droplet-mediated kinetic-to-thermodynamic transition

Phase transitions of conjugated polymers into solid states typically require elevated temperatures.[43–45] However, in this study, we observed that the phase transition of P(T-PEG$_3$)$_{25}$ in THF/EtOH (Fig. 2a) or THF/H$_2$O (Fig. 2e) solutions occurs under mild conditions. To elucidate the role of the liquid-like intermediate in the kinetically controlled nonequilibrium self-assembly, we investigated the droplet-mediated KTT process in detail. Fig. 1c clearly shows the formation of an intermediate state that bridges the initially KTAs and the final thermodynamically favored structures, where, during thermal treatment
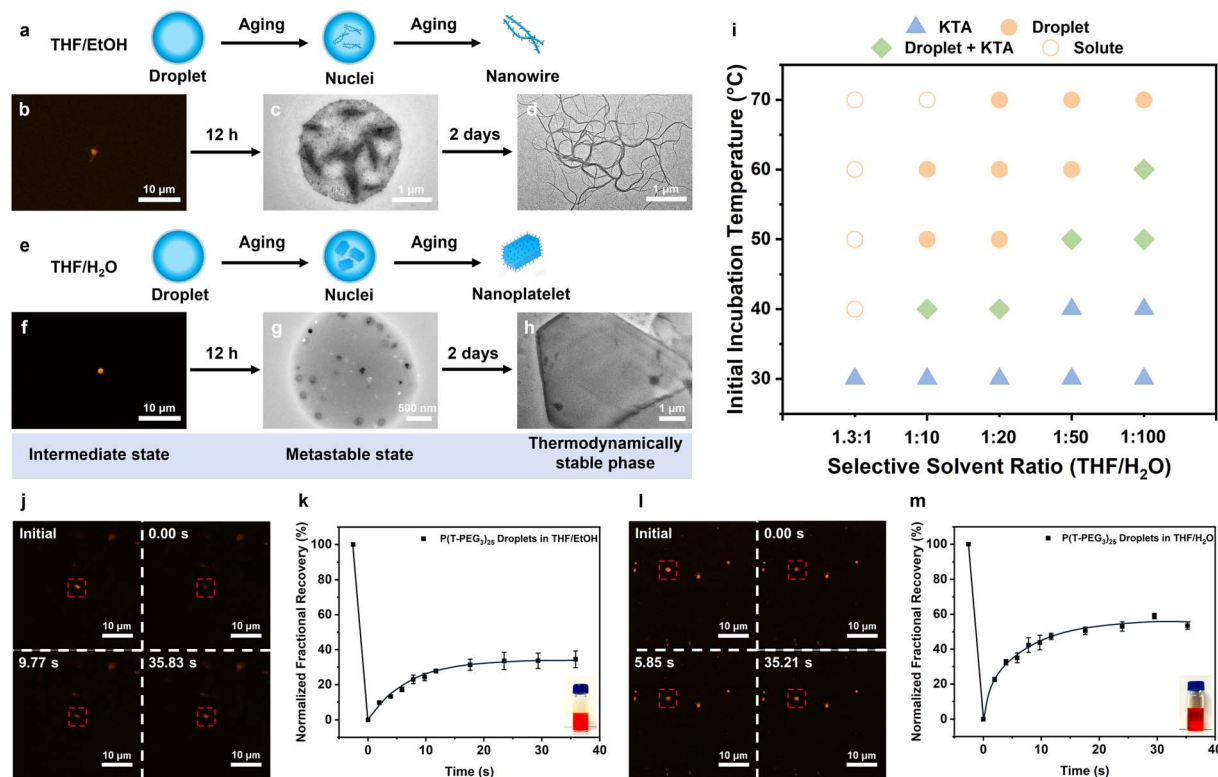
Fig. 2 Phase transformation of P(T-PEG$_3$)$_{25}$ nanoparticles from KTAs to different morphologies. (a) Schematic illustration of phase transformation forming wire-like nanoparticles. CLSM and TEM micrographs of (b) liquid-like droplets, (c) the coexistence of both liquid and solid phases, and (d) wire-like nanoparticles in the THF/EtOH solution. (e) Schematic illustration of phase transformation forming plate-like nanoparticles. CLSM and TEM micrographs of (f) liquid-like droplets, (g) the coexistence of both liquid and solid phases, and (h) plate-like nanoparticles in the THF/H$_2$O solution. (i) Condition matrices of nanoparticles through different self-assembly pathways in the THF/EtOH solution. FRAP (j) images of temporal recovery and corresponding (k) recovery profile of thiophene-based liquid-like droplets in the THF/H$_2$O solution. FRAP (l) images of temporal recovery and corresponding (m) recovery profile of thiophene-based liquid-like droplets in the THF/EtOH solution. Scale bar = 10 μm for (b, f, j, and l), 1 μm for (c, d, and h), 500 nm for (g).

of P(T-PEG$_3$)$_{25}$ KTAs in THF/H$_2$O within 12 h, a new broad Gaussian-shaped absorption band appeared, centered at 503 nm (λ_{max} = 2.46 eV). This band was markedly different from the vibronically resolved spectra of both the initial KTAs and the final 2D nanoplatelet assemblies. Concomitant with the emergence of the 503 nm absorption, a cloudy red suspension formed upon heating the initially clear orange KTA solution, which reverted to a transparent orange state upon cooling. A similar intermediate phase was also observed in the THF/EtOH system. However, in contrast to THF/H$_2$O, the absorption spectra of the intermediate in THF/EtOH remained Gaussian-like and closely resembled those of both the KTAs and the final 1D nanowires (Fig. 1b), indicating minimal changes in molecular ordering.

Optical microscopy and TEM revealed that these transient intermediates in both solvent systems adopt spherical morphologies (Fig. S5a–d), which are different from those of the initial KTAs and the final anisotropic assemblies. Taking advantage of the intrinsic fluorescence of P(T-PEG$_3$)$_{25}$, confocal laser scanning microscopy (CLSM) confirmed the morphologies of these intermediates (Fig. 2b and f). Fluorescence recovery after photobleaching (FRAP) experiments further substantiated their liquid-like nature. As shown in Fig. 2k and m,

photobleaching a selected region within a droplet led to rapid fluorescence recovery within approximately 40 seconds. Interestingly, although the liquid-like intermediates in both solvent systems exhibited fast recovery dynamics, the recovery efficiency in the THF/H$_2$O system (~60%) was markedly higher than that in THF/EtOH (~35%), suggesting a more fluidic and dynamic nature of the P(T-PEG$_3$)$_{25}$ intermediates in the more polar, water-containing environment.

The hydrophilicity of conjugated homopolymers plays a critical role in the formation of liquid-like intermediates. To elucidate the role of polar side chains, we examined the self-assembly behavior of polythiophenes with PEG side chains of varying lengths. The polymer P(T-PEG$_2$)$_{23}$, which contains short PEG$_2$ side chains, exhibited rapid macroscopic phase separation in a THF/H$_2$O (1 : 20 v/v) mixture at RT. When heated to 60 °C, the phase-separated polymers rapidly precipitated from the solution without the formation of liquid-like intermediates (Fig. S6a and b). This behavior can be attributed to the weaker hydrogen bonding interactions of the shorter PEG$_2$ side chains with water, in contrast to the more extended PEG$_3$ chains present in P(T-PEG$_3$)$_{25}$. It indicated that strong hydrogen-bonding networks between the side chains and the solvent are
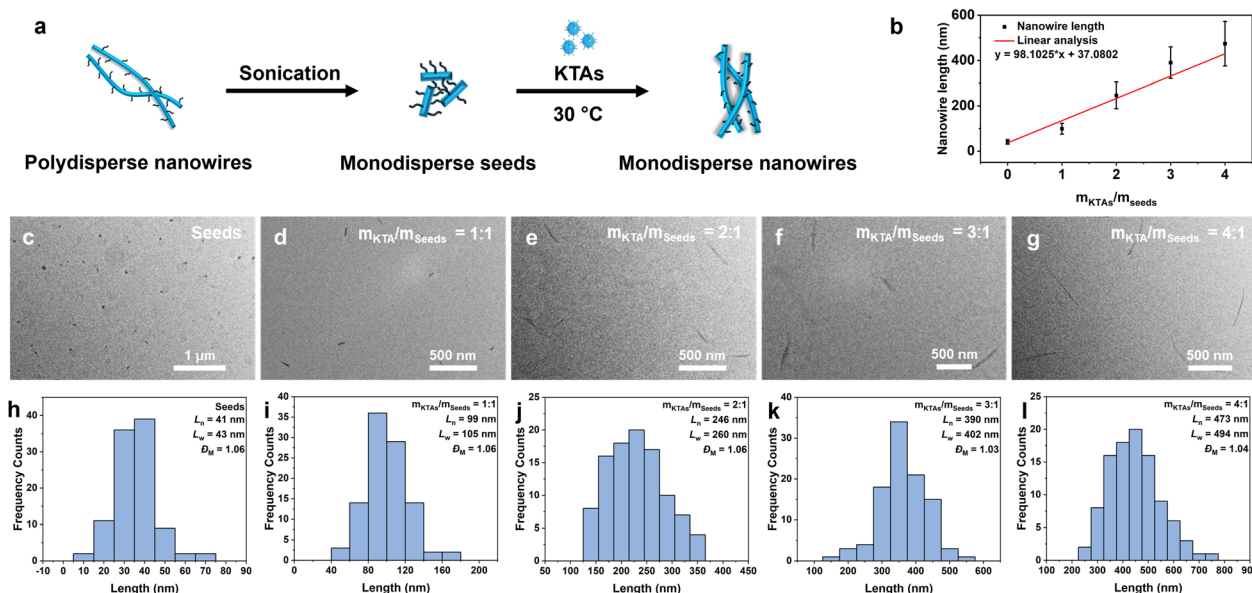
Fig. 3 Seeded growth of furan-based nanowires. (a) Schematic illustration of the seeded growth of $P(F-PEG_3)_{22}$ homopolymers for forming nanowires. (b) Linear seeded growth of nanowires with narrow length dispersity. TEM micrographs of (c) low-dispersity seed micelles and nanowires with different unimer-to-seed ratios (d) 1 : 1, (e) 2 : 1, (f) 3 : 1, (g) 4 : 1. Corresponding distribution profiles of (h) seeds and nanowires with different unimer-to-seed ratios (i) 1 : 1, (j) 2 : 1, (k) 3 : 1, (l) 4 : 1. Scale bar = 1 μm for (c), 500 nm for (d−g).

essential for stabilizing intermediate liquid-like states during the assembly process.

It is well established that the morphological reorganization of certain small molecules can proceed via metastable liquid–liquid phase separation (LLPS).[46] In order to investigate the transformation behavior of $P(T-PEG_3)_{25}$ polymers from the intermediate droplet state to the thermodynamically favored morphology, we monitored the structural evolution of the droplets under continuous heating. TEM analysis revealed that nucleation could occur within the liquid-like intermediates. Specifically, when 0.5 mg mL^{-1} THF/H$_2$O (1 : 20, v/v) KTAs solution and 0.2 mg mL^{-1} THF/EtOH (1 : 50, v/v) KTAs solution were heated at 60 °C for 12 h and then slowly cooled to room temperature over 6 h and 12 h, respectively, small nanosheets and nanowire nucleation sites began to emerge within the fused droplets. As shown in Fig. 2c and g, TEM images with caution of the drying effect demonstrated the existence of both the small nanosheets and nanowire nucleation sites. Subsequent aging at RT facilitated the gradual growth of these nuclei. After aging for 2 days, this process eventually drove a complete phase transition from a mixed liquid–solid state to well-defined 1D wire-like structures in the THF/EtOH system (Fig. 2d) and 2D plate-like structures in the THF/H$_2$O system (Fig. 2h). Notably, slow cooling was found to be crucial for the formation of well-ordered nanostructures. To further elucidate this effect, a control experiment was conducted: a 0.5 mg mL^{-1} THF/H$_2$O (1 : 20, v/v) KTAs solution was heated at 60 °C for 12 h and then rapidly cooled in an ice–water bath to 0 °C within 3 min. In this case, no well-defined nanoplatelets were observed; instead, irregularly shaped aggregates were obtained (Fig. S7a and b). We attribute this result to the rapid loss of fluidity in the

intermediates during fast cooling, which prevents the system from reorganizing into ordered nanostructures.

To highlight the role of the intermediate droplet state in directing the formation of 1D and 2D assemblies, we also examined how different assembly pathways influence the resulting morphology. We found that solution concentration exerted a negligible influence on droplet formation, as KTAs at various concentrations produced similar nanowire and nano-sheet morphologies under identical solvent compositions (Fig. S8a–d). In contrast, varying the solvent composition had a pronounced effect on droplet formation. As shown in Fig. 2i and S9–S13, increasing the solvent polarity raised the temperature required to induce droplet formation, while decreasing the polarity resulted in KTA dissolution upon heating. We chose THF/EtOH (1 : 1 v/v) and THF/H$_2$O (1.3 : 1 v/v) mixtures as representative systems, where $P(T-PEG_3)_{25}$ KTAs readily formed at RT. Upon heating to 60 °C, these aggregates completely dissolved. Temperature-dependent UV-vis spectroscopy confirmed this process and showed that slow cooling triggered partial reassembly of the polymers (Fig. S14). However, after 2 days of aging, well-defined nanowires or nanoplatelets were not formed through this route. These results indicate that the dissolution–reassembly process follows a distinct assembly pathway, leading to structural outcomes significantly different from those observed in the droplet-mediated KTT.

Seed-assisted kinetic-to-thermodynamic transition for nanowires and nanoplatelets

While living CDSA has been highly effective for π-conjugated block copolymers,[6,47–52] its extension to conjugated homopolymers has been hindered by poor colloidal stability and rapid,
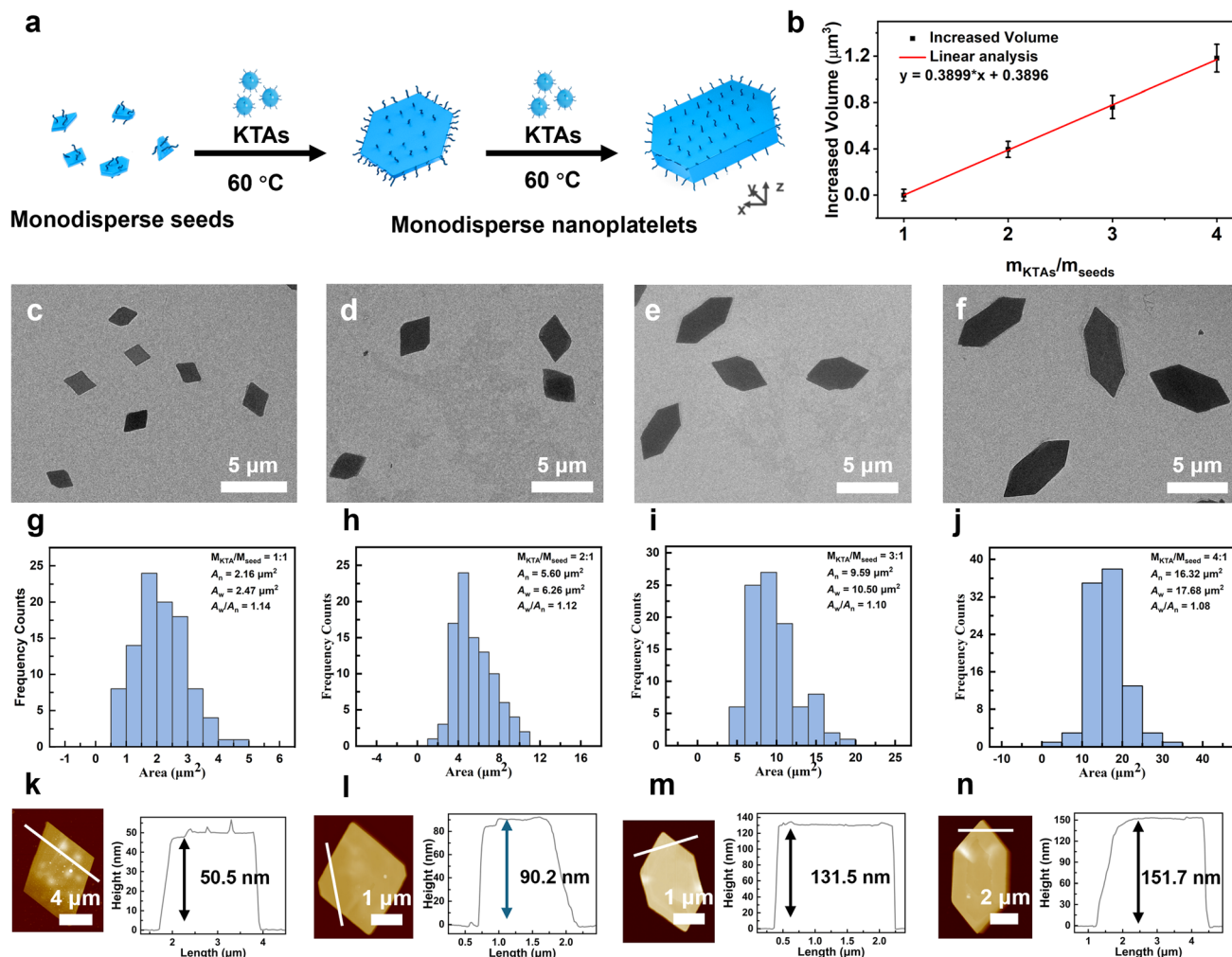
Fig. 4 Seeded growth of furan-based nanoplatelets. (a) Schematic illustration of the seeded growth of $P(F-PEG_3)_{22}$ homopolymers for forming nanoplatelets. (b) Linear seeded growth of nanoplatelets with narrow volume dispersity. TEM micrographs of plate-like micelles with different unimer-to-seed ratios (c) 1 : 1, (d) 2 : 1, (e) 3 : 1, (f) 4 : 1. Corresponding distribution profiles of nanoplatelets with different unimer-to-seed ratios (g) 1 : 1, (h) 2 : 1, (i) 3 : 1, (j) 4 : 1. Corresponding AFM micrographs and height profiles of nanoplatelets with different unimer-to-seed ratios (k) 1 : 1, (l) 2 : 1, (m) 3 : 1, (n) 4 : 1, measured along the solid line denoted in white. Scale bar = 5 μm for (c–f), 4 μm for (k), 2 μm for (n), 1 μm for (l and m).

uncontrolled aggregation under kinetic control.[31,53] On the basis of the above studies, we aim to explore whether seed-assisted KTT can be harnessed as a viable pathway to enable living CDSA of conjugated homopolymers.

To this end, we first prepared morphologically pure 1D nanowires or 2D nanoplatelets of a conjugated homopolymer, followed by sonication to generate seeds. These seeds were then introduced into solutions containing KTAs to evaluate their influence on the seed-assisted KTT strategy. Notably, in addition to polythiophene, we found other conjugated homopolymers, such as polyfuran (PF), also exhibited similar droplet-mediated KTT behavior (Fig. S15–S17), highlighting the versatility of this approach and expanding the toolkit for living self-assembly studies. Comparative analysis revealed that poly[3-(2-(2-(2-methoxyethoxy)ethoxy)ethoxy)methylfuran] [(P(F-PEG$_3$)$_{22}$], $M_n = 5.25$ kg mol^{-1}, $Đ_M = 1.50$) formed wire-like seeds with significantly enhanced crystallinity in THF/EtOH mixtures compared to P(T-PEG$_3$)$_{25}$. As shown in Fig. 3c and h, the

resulting seeds of P(F-PEG$_3$)$_{22}$ exhibited an average length of *ca.* 41 nm and a dispersity ($Đ_M$) of 1.06. These preformed KTAs (0.2 mg mL^{-1} in THF/EtOH, 1 : 50 v/v, Fig. S16a) were subsequently mixed with the 1D seeds (0.01 mg mL^{-1}) in the same THF/EtOH solvent at RT in specified mass ratios ($m_{KTAs} : m_{seeds} = 1, 2, 3$, and 4) by gentle shaking for 30 s. The resulting solutions were then aged for 48 h at 30 °C. To verify 1D seed stability, a control sample containing only the seed solution was subjected to the same thermal conditions. After 2 days, TEM analysis confirmed negligible morphological changes in the control group. In contrast, the samples undergoing seeded growth yielded low-dispersity wire-like structures with well-controlled lengths linearly ranging from 99 ± 24 to 474 ± 98 nm (Fig. 3b, d–g, i–l, and Table S3). These results demonstrate that seed-assisted KTT enables living 1D assembly of conjugated homopolymers in solution.

In the case of 2D living self-assembly, monodisperse 2D seeds were generated by sonicating polydisperse P(F-PEG$_3$)$_{22}$
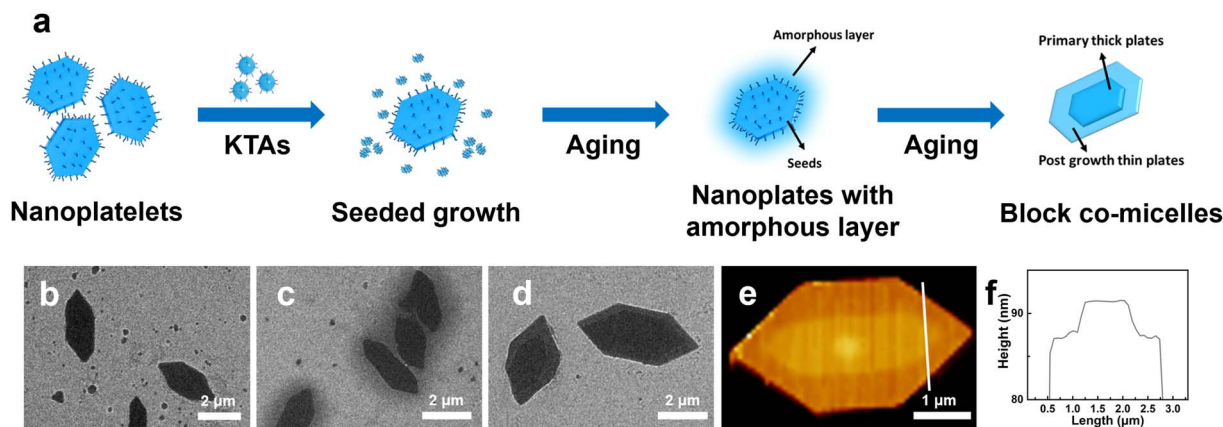
Fig. 5 Seeded growth pathways with different monomers for forming block co-micelles. (a) Schematic illustration of the seeded growth of P(F-PEG$_3$)$_{22}$ homopolymers for forming block co-micelles. Corresponding TEM and AFM micrographs of (b) the mixture of nanoplatelets and KTAs, (c) nanoplatelets with amorphous layers, (d and e) block co-micelles, (f) the height profile of the block co-micelle. Scale bar = 2 µm for (b–d), 1 µm for (e).

naoplatelets in a THF/H$_2$O mixture (1 : 20 v/v), affording a number-average area (A_n) of 0.18 µm^2 and a dispersity ($Đ_M$) of 2.07 (Fig. S18a and b). These 2D seeds (0.01 mg mL^{-1}) were then mixed with preformed KTAs of P(F-PEG$_3$)$_{22}$ (0.5 mg mL^{-1} in THF/H$_2$O, 1 : 20 v/v, Fig. S16f) in the same THF/H$_2$O solvent at RT in specified mass ratios (m_{KTAs} : m_{seeds} = 1, 2, 3, and 4) by gentle shaking for 30 s, followed by aging at 60 °C. To confirm the stability of the 2D seeds, a control experiment was performed by subjecting the seed solution alone to identical aging conditions at 60 °C for 48 h. TEM imaging revealed no appreciable morphological alterations in the control sample. In contrast, samples containing a mixture of 2D seeds and KTAs yielded uniform hexagonal nanoplatelets. As shown in Fig. 4c–f, increasing the KTA-to-seed ratio led to a progressive enlargement of the nanoplatelets, with average areas of 2.16, 5.60, 9.59, and 16.32 µm^2, respectively, and narrow dispersity (A_w/A_n) from 1.14 to 1.08 (Fig. 4g–j and Table S4). Interestingly, in contrast to conventional 2D self-assembly of block copolymers—where the height of the nanoplatelets typically remains constant during seeded growth[54–56]—AFM measurements revealed a substantial increase in nanoplatelet height from approximately 50 nm to 150 nm as the assembly proceeded (Fig. 4k–n). Motivated by the observed three-dimensional (3D) growth mode, we further examined the living character of the seeded growth and found that the volume of the resulting platelets exhibited a linear correlation with the KTA-to-seed mass ratio (Fig. 4b), clearly demonstrating 3D living growth behavior.

Grazing-incidence wide-angle X-ray scattering (GIWAXS) measurements (Fig. S19a) revealed the crystalline nature of the assembled 2D nanoplatelets. As shown in Fig. S19b, distinct (100) and (200) reflections were observed along the out-of-plane direction, indicating an edge-on arrangement of polymer backbones, reminiscent of crystalline polythiophene thin films.[57] An in-plane (010) reflection at Q = 1.5120 Å^{-1} corresponds to a π–π stacking distance of 0.41 nm, confirming that the π–π stacking direction is aligned parallel to the substrate. The out-of-plane d-spacing of the layered structure was

determined to be 1.88 nm (Fig. S19c). The short interlayer distance suggests strong van der Waals interactions between the polyethylene glycol side chains, which may facilitate the vertical growth of the nanoplatelets. High-resolution AFM imaging further confirmed the presence of a layered architecture, with each layer measuring approximately 3.5 nm in thickness (Fig. S19d). This value aligns with the simulated molecular width of P(F-PEG$_3$)$_{22}$ (3.16 nm), supporting the notion that out-of-plane growth arises from interchain interactions among the PEG side chains.

It is well established that polymer solubility plays a key role in the crystallization rate of living CDSA.[58–60] However, in this system, P(F-PEG$_3$)$_{22}$ remained insoluble in THF/H$_2$O (1 : 20 v/v), even during assembly. To investigate the mechanism of the seed-assisted KTT, we monitored the seeded growth process (Fig. 5a). KTAs of P(F-PEG$_3$)$_{22}$ were mixed with uniform 2D seeds, and both species could be clearly identified at the early stage (Fig. 5b). After 2 h of heating, the surfaces of the 2D crystalline seeds were coated with amorphous polymer (Fig. 5c), suggesting that liquid-like intermediates may surround and adhere to the 2D crystalline seeds due to the heating process. This coating appears to play a key role in enabling uniform crystal growth across the nanoplatelet surface. Upon prolonged heating, the amorphous coating gradually vanished, yielding large, fully crystalline 2D nanoplatelets (Fig. 5d). Interestingly, the thickness of the outer nanoplatelet domains could be tuned by lowering the growth temperature. This approach produced block co-crystals with distinct inner and outer thicknesses (Fig. 5e and f), indicating that the seed-assisted KTT offers a stepwise and controllable assembly strategy.

Conclusions

In summary, we have developed a versatile strategy for preparing well-defined nanostructures of π-conjugated homopolymers through kinetically controlled nonequilibrium self-assembly. The central concept is to introduce stable, liquid-

like intermediates during the kinetic-to-thermodynamic transition (KTT) from kinetically favored metastable assemblies, such as kinetically trapped assemblies (KTAs), to thermodynamically favored form transition, such as nanowires or nanoplatelets. This process involves (i) converting rigid, solid KTAs into dynamic, liquid-like intermediates, and (ii) directing nucleation and seeded growth within these liquid-like intermediates toward thermodynamically favored morphologies. Using this droplet-mediated KTT approach, we obtained a series of highly uniform 1D wire-like structures and 2D plate-like structures from conjugated homopolymers. The liquid-like intermediates generated during the transition proved essential for achieving precise morphological control. A key advantage of this method is that the solvent environment can be tuned to regulate nucleation within the liquid-like intermediates, thereby enabling fine control over the final thermodynamically favored morphology of a given polymer. Furthermore, the fluidity of the intermediates allows seeded growth, leading to size-controlled nanostructures. By introducing either 1D or 2D seeds, we produced dimensionally uniform nanowires and nanoplatelets spanning sizes from tens of nanometers to several micrometers. This strategy provides critical insights into the programmable kinetically controlled nonequilibrium self-assembly of π-conjugated polymers and offers a powerful approach for tailoring their structure, morphology, and dimensions through controlled phase transitions.

Author contributions

Z. Li: conceptualization, data curation, formal analysis, investigation (lead), methodology, resources, validation (lead), visualization (lead), writing – original draft, writing – review & editing. Y. Gu: investigation (supporting), visualization (supporting). Y. Liu: investigation (supporting), validation (supporting). S. Ji: investigation (supporting). X. Jin: conceptualization, funding acquisition, resources, supervision, writing – review & editing.

Conflicts of interest

There are no conflicts to declare.

Data availability

The authors have cited additional references within the supporting information (SI).[41,42,61–69] Supplementary information: materials and methods, characterization methods and SI data. See DOI: https://doi.org/10.1039/d5sc06844d.

Acknowledgements

References

1 G. E. J. Hicks, S. Li, N. K. Obhi, C. N. Jarrett-Wilkins and D. S. Seferos, Programmable Assembly of π-Conjugated Polymers, *Adv. Mater.*, 2021, **33**, 2006287.

2 L. Bai, N. Wang and Y. Li, Controlled Growth and Self-Assembly of Multiscale Organic Semiconductor, *Adv. Mater.*, 2022, **34**, 2102811.

3 L. R. MacFarlane, H. Shaikh, J. D. Garcia-Hernandez, M. Vespa, T. Fukui and I. Manners, Functional nanoparticles through π-conjugated polymer self-assembly, *Nat. Rev. Mater.*, 2021, **6**, 7–26.

4 L. MacFarlane, C. Zhao, J. Cai, H. Qiu and I. Manners, Emerging applications for living crystallization-driven self-assembly, *Chem. Sci.*, 2021, **12**, 4661–4682.

5 A. K. Pearce, T. R. Wilks, M. C. Arno and R. K. O'Reilly, Synthesis and applications of anisotropic nanoparticles with precisely defined dimensions, *Nat. Rev. Chem.*, 2021, **5**, 21–45.

6 X.-H. Jin, M. B. Price, J. R. Finnegan, C. E. Boott, J. M. Richter, A. Rao, S. M. Menke, R. H. Friend, G. R. Whittell and I. Manners, Long-range exciton transport in conjugated polymer nanofibers prepared by seeded growth, *Science*, 2018, **360**, 897–900.

7 L. Ye, X. Jiao, M. Zhou, S. Zhang, H. Yao, W. Zhao, A. Xia, H. Ade and J. Hou, Manipulating Aggregation and Molecular Orientation in All-Polymer Photovoltaic Cells, *Adv. Mater.*, 2015, **27**, 6046–6054.

8 Z.-F. Yao, Y.-Q. Zheng, J.-H. Dou, Y. Lu, Y.-F. Ding, L. Ding, J.-Y. Wang and J. Pei, Approaching Crystal Structure and High Electron Mobility in Conjugated Polymer Crystals, *Adv. Mater.*, 2021, **33**, 2006794.

9 H. Dong and W. Hu, Multilevel Investigation of Charge Transport in Conjugated Polymers, *Acc. Chem. Res.*, 2016, **49**, 2435–2443.

10 Z. Li, H. Guo and X. Jin, Fabrication of Uniform Anionic Polymeric Nanoplatelets as Building Blocks for Constructing Conductive Hydrogels with Enhancing Conductive and Mechanical Properties, *Macromol. Rapid Commun.*, 2024, **45**, 2400008.

11 H. Fu, Z. Peng, Q. Fan, F. R. Lin, F. Qi, Y. Ran, Z. Wu, B. Fan, K. Jiang, H. Y. Woo, G. Lu, H. Ade and A. K.-Y. Jen, A Top-Down Strategy to Engineer ActiveLayer Morphology for Highly Efficient and Stable All-Polymer Solar Cells, *Adv. Mater.*, 2022, **34**, 2202608.

12 Z. Li, A. K. Pearce, J. Du, A. P. Dove and R. K. O'Reilly, Uniform antibacterial cylindrical nanoparticles for enhancing the strength of nanocomposite hydrogels, *J. Polym. Sci.*, 2023, **61**, 44–55.

13 H. C. Parkin, J. D. Garcia-Hernandez, S. T. G. Street, R. Hof and I. Manners, Uniform, length-tunable antibacterial 1D diblock copolymer nanofibers, *Polym. Chem.*, 2022, **13**, 2941–2949.

14 M. C. Arno, M. Inam, A. C. Weems, Z. Li, A. L. A. Binch, C. I. Platt, S. M. Richardson, J. A. Hoyland, A. P. Dove and R. K. O'Reilly, Exploiting the role of nanoparticle shape in

enhancing hydrogel adhesive and mechanical properties, *Nat. Commun.*, 2020, **11**, 1420.

15 Z. Li, A. K. Pearce, A. P. Dove and R. K. O'Reilly, Precise Tuning of Polymeric Fiber Dimensions to Enhance the Mechanical Properties of Alginate Hydrogel Matrices, *Polymers*, 2021, **13**, 2202.

16 C. Clamor, S. D. Dale, J. Beament, E. Mould, R. K. O'Reilly and A. P. Dove, Uniform Polyester-Based Nanoparticles Assembled *via* Living Crystallization-Driven Self-Assembly as Friction-Reducing Agents in Engine Oil, *Macromolecules*, 2023, **56**, 9821–9828.

17 S. D. P. Fielden, Kinetically Controlled and Nonequilibrium Assembly of Block Copolymers in Solution, *J. Am. Chem. Soc.*, 2024, **146**, 18781–18796.

18 S. Ganda and M. H. Stenzel, Concepts, fabrication methods and applications of living crystallization-driven self-assembly of block copolymers, *Prog. Polym. Sci.*, 2020, **101**, 101195.

19 J. Ma, G. Lu, X. Huang and C. Feng, π-Conjugated-polymer-based nanofibers through living crystallization-driven self-assembly: preparation, properties and applications, *Chem. Commun.*, 2021, **57**, 13259–13274.

20 J. Gu, Z. Chu, B. Zheng and Z. Tong, Design of Precise Nanoparticles *via* Polymer Crystallization, *ACS Macro Lett.*, 2025, **14**, 645–657.

21 Z. Gao, X. Zhang, B. Zheng, J. Gu and Z. Tong, Creation of Segmented Platelets with Diverse Crystalline Cores Using Double Crystalline Triblock Copolymers, *J. Am. Chem. Soc.*, 2025, **147**, 5172–5181.

22 F. Teng, J. Gu, Z. Chu and Z. Tong, Lateral Growth of Hexagonal Platelet Micelles *via* Crystallization by Particle Attachment, *Macromolecules*, 2025, **58**, 249–255.

23 M. C. Arno, M. Inam, Z. Coe, G. Cambridge, L. J. Macdougall, R. Keogh, A. P. Dove and R. K. O'Reilly, Precision Epitaxy for Aqueous 1D and 2D Poly(ε-caprolactone) Assemblies, *J. Am. Chem. Soc.*, 2017, **139**, 16980–16985.

24 X. Zhang, G. Chen, L. Liu, L. Zhu and Z. Tong, Precise Control of Two-Dimensional Platelet Micelles from Biodegradable Poly(p-dioxanone) Block Copolymers by Crystallization-Driven Self-Assembly, *Macromolecules*, 2022, **55**, 8250–8261.

25 S. Pearce, H. K. MacKenzie, H. Shaikh, Z. Liu, R. Harniman, J. C. Eloi, S. Davis, R. M. Richardson, E. A. LaPierre, I. Manners and Y. Zhang, Probing the Heteroepitaxial Seeded Growth and Self-Sorting Processes of Segmented Co-Micelles with Chemically Distinct Crystalline Cores, *Angew. Chem., Int. Ed.*, 2025, **64**, e202506872.

26 Y. He, J.-C. Eloi, R. L. Harniman, R. M. Richardson, G. R. Whittell, R. T. Mathers, A. P. Dove, R. K. O'Reilly and I. Manners, Uniform Biodegradable Fiber-Like Micelles and Block Comicelles *via* "Living" Crystallization-Driven Self-Assembly of Poly(l-lactide) Block Copolymers: The Importance of Reducing Unimer Self-Nucleation *via* Hydrogen Bond Disruption, *J. Am. Chem. Soc.*, 2019, **141**, 19088–19098.

27 X. Wang, G. Guerin, H. Wang, Y. Wang, I. Manners and M. A. Winnik, Cylindrical block copolymer micelles and

co-micelles of controlled length and architecture, *Science*, 2007, **317**, 644–647.

28 J. B. Gilroy, T. Gädt, G. R. Whittell, L. Chabanne, J. M. Mitchels, R. M. Richardson, M. A. Winnik and I. Manners, Monodisperse cylindrical micelles by crystallization-driven living self-assembly, *Nat. Chem.*, 2010, **2**, 566–570.

29 S.-H. Hwang, S.-Y. Kang, S. Yang, J. Lee and T.-L. Choi, Synchronous preparation of length-controllable 1D nanoparticles *via* crystallization-driven *in situ* nanoparticlization of conjugated polymers, *J. Am. Chem. Soc.*, 2022, **144**, 5921–5929.

30 D. Yao, Y. Zhang, X. Zhou, X. Sun, X. Liu, J. Zhou, W. Jiang, W. Hua and H. Liang, Catalytic-assembly of programmable atom equivalents, *Proc. Natl. Acad. Sci. U. S. A.*, 2023, **120**, e2219034120.

31 T. Fukui, J. D. Garcia-Hernandez, L. R. MacFarlane, S. Lei, G. R. Whittell and I. Manners, Seeded Self-Assembly of Charge-Terminated Poly(3-hexylthiophene) Amphiphiles Based on the Energy Landscape, *J. Am. Chem. Soc.*, 2020, **142**, 15038–15048.

32 F. J. Esselink, E. E. Dormidontova and G. Hadziioannou, Redistribution of Block Copolymer Chains between Mixed Micelles in Solution, *Macromolecules*, 1998, **31**, 4873–4878.

33 S. Cerritelli, A. Fontana, D. Velluto, M. Adrian, J. Dubochet, P. De Maria and J. A. Hubbell, Thermodynamic and Kinetic Effects in the Aggregation Behavior of a Poly(ethylene glycol-b-propylene sulfide-b-ethylene glycol) ABA Triblock Copolymer, *Macromolecules*, 2005, **38**, 7845–7851.

34 P. A. Korevaar, S. J. George, A. J. Markvoort, M. M. J. Smulders, P. A. J. Hilbers, A. P. H. J. Schenning, T. F. A. De Greef and E. W. Meijer, Pathway complexity in supramolecular polymerization, *Nature*, 2012, **481**, 492–496.

35 E. Mattia and S. Otto, Supramolecular systems chemistry, *Nat. Nanotechnol.*, 2015, **10**, 111–119.

36 S. Ogi, K. Sugiyasu, S. Manna, S. Samitsu and M. Takeuchi, Living supramolecular polymerization realized through a biomimetic approach, *Nat. Chem.*, 2014, **6**, 188–195.

37 I. D. Tevis, L. C. Palmer, D. J. Herman, I. P. Murray, D. A. Stone and S. I. Stupp, Self-Assembly and Orientation of Hydrogen-Bonded Oligothiophene Polymorphs at Liquid–Membrane–Liquid Interfaces, *J. Am. Chem. Soc.*, 2011, **133**, 16486–16494.

38 A. Sorrenti, J. Leira-Iglesias, A. J. Markvoort, T. F. A. de Greef and T. M. Hermans, Non-equilibrium supramolecular polymerization, *Chem. Soc. Rev.*, 2017, **46**, 5476–5490.

39 Q. Wang, Z. Qi, M. Chen and D.-H. Qu, Out-of-equilibrium supramolecular self-assembling systems driven by chemical fuel, *Aggregate*, 2021, **2**, e110.

40 N. Yun, C. Kang, S. Yang, S.-H. Hwang, J.-M. Park and T.-L. Choi, Size-tunable semiconducting 2D nanorectangles from conjugated polyenyne homopolymer synthesized *via* cascade metathesis and metallotropy polymerization, *J. Am. Chem. Soc.*, 2023, **145**, 9029–9038.

41 H. Duijs, M. Kumar, S. Dhiman and L. Su, Harnessing competitive interactions to regulate supramolecular

"micelle-droplet-fiber" transition and reversibility in water, *J. Am. Chem. Soc.*, 2024, **146**, 29759–29766.

42 G. Vantomme, G. M. Ter Huurne, C. Kulkarni, H. M. Ten Eikelder, A. J. Markvoort, A. R. Palmans and E. Meijer, Tuning the length of cooperative supramolecular polymers under thermodynamic control, *J. Am. Chem. Soc.*, 2019, **141**, 18278–18285.

43 A. Rodrigues, M. C. R. Castro, A. S. F. Farinha, M. Oliveira, J. P. C. Tomé, A. V. Machado, M. M. M. Raposo, L. Hilliou and G. Bernardo, Thermal stability of P3HT and P3HT:PCBM blends in the molten state, *Polym. Test.*, 2013, **32**, 1192–1201.

44 J. Martín, A. Nogales and M. Martín-González, The Smectic–Isotropic Transition of P3HT Determines the Formation of Nanowires or Nanotubes into Porous Templates, *Macromolecules*, 2013, **46**, 1477–1483.

45 A. J. Pearson, T. Wang, R. A. L. Jones, D. G. Lidzey, P. A. Staniec, P. E. Hopkinson and A. M. Donald, Rationalizing Phase Transitions with Thermal Annealing Temperatures for P3HT:PCBM Organic Photovoltaic Devices, *Macromolecules*, 2012, **45**, 1499–1508.

46 S. Patra, S. Chandrabhas, S. Dhiman and S. J. George, Controlled Supramolecular Polymerization *via* Bioinspired, Liquid–Liquid Phase Separation of Monomers, *J. Am. Chem. Soc.*, 2024, **146**, 12577–12586.

47 C. Wang, F. Huang, X. Huang, G. Lu and C. Feng, Precision Preparation of π-Conjugated-Polymer-Based Nanofibers with Shell Tailorability by Combining Living Crystallization-Driven Self-Assembly with Nitrile N-Oxide-Based Cycloaddition, *Macromolecules*, 2025, **58**, 4790–4806.

48 J. Nie, X. Huang, G. Lu, M. A. Winnik and C. Feng, Living Crystallization-Driven Self-Assembly of Linear and V-Shaped Oligo(p-phenylene ethynylene)-Containing Block Copolymers: Architecture Effect of π-Conjugated Crystalline Segment, *Macromolecules*, 2022, **55**, 7856–7868.

49 J. Nie, Z. Wang, X. Huang, G. Lu and C. Feng, Uniform Continuous and Segmented Nanofibers Containing a π-Conjugated Oligo(p-phenylene ethynylene) Core *via* "Living" Crystallization-Driven Self-Assembly: Importance of Oligo(p-phenylene ethynylene) Chain Length, *Macromolecules*, 2020, **53**, 6299–6313.

50 O. El-Zubir, E. L. Kynaston, J. Gwyther, A. Nazemi, O. E. C. Gould, G. R. Whittell, B. R. Horrocks, I. Manners and A. Houlton, Bottom-up device fabrication *via* the seeded growth of polymer-based nanowires, *Chem. Sci.*, 2020, **11**, 6222–6228.

51 U. Tritschler, J. Gwyther, R. L. Harniman, G. R. Whittell, M. A. Winnik and I. Manners, Toward Uniform Nanofibers with a π-Conjugated Core: Optimizing the "Living" Crystallization-Driven Self-Assembly of Diblock Copolymers with a Poly(3-octylthiophene) Core-Forming Block, *Macromolecules*, 2018, **51**, 5101–5113.

52 E. L. Kynaston, A. Nazemi, L. R. MacFarlane, G. R. Whittell, C. F. J. Faul and I. Manners, Uniform Polyselenophene Block Copolymer Fiberlike Micelles and Block Co-micelles *via* Living Crystallization-Driven Self-Assembly, *Macromolecules*, 2018, **51**, 1002–1010.

53 S. Yang, S.-Y. Kang and T.-L. Choi, Semi-conducting 2D rectangles with tunable length *via* uniaxial living crystallization-driven self-assembly of homopolymer, *Nat. Commun.*, 2021, **12**, 2602.

54 X. Yu, Y. Fang, Z. Luo, X. Guo, L. Fu, Z. Fan, J. Zhao, H. Xie, M. Guo and B. Cheng, Precise Preparation of Size-Uniform Two-Dimensional Platelet Micelles Through Crystallization-Assisted Rapid Microphase Separation Using All-Bottlebrush-Type Block Copolymers with Crystalline Side Chains, *J. Am. Chem. Soc.*, 2025, **147**, 2193–2205.

55 S. Pearce, X. He, M.-S. Hsiao, R. L. Harniman, L. R. MacFarlane and I. Manners, Uniform, High-Aspect-Ratio, and Patchy 2D Platelets by Living Crystallization-Driven Self-Assembly of Crystallizable Poly(ferrocenyldimethylsilane)-Based Homopolymers with Hydrophilic Charged Termini, *Macromolecules*, 2019, **52**, 6068–6079.

56 A. Nazemi, X. He, L. R. MacFarlane, R. L. Harniman, M.-S. Hsiao, M. A. Winnik, C. F. Faul and I. Manners, Uniform "patchy" platelets by seeded heteroepitaxial growth of crystallizable polymer blends in two dimensions, *J. Am. Chem. Soc.*, 2017, **139**, 4409–4417.

57 O. Dolynchuk, R. T. Kahl, F. Meichsner, A. J. Much, A. Pechevystyi, A. Averkova, A. Erhardt, M. Thelakkat and T. Thurn-Albrecht, Controlling Crystal Orientation in Films of Conjugated Polymers by Tuning the Surface Energy, *Macromolecules*, 2024, **57**, 10399–10409.

58 C. E. Boott, E. M. Leitao, D. W. Hayward, R. F. Laine, P. Mahou, G. Guerin, M. A. Winnik, R. M. Richardson, C. F. Kaminski, G. R. Whittell and I. Manners, Probing the Growth Kinetics for the Formation of Uniform 1D Block Copolymer Nanoparticles by Living Crystallization-Driven Self-Assembly, *ACS Nano*, 2018, **12**, 8920–8933.

59 M. Vespa, Z. M. Hudson and I. Manners, Homogeneous and Segmented Nanofibers with a Conjugated Poly[3-(2′-ethylhexyl)thiophene] Core *via* Living Crystallization-Driven Self-Assembly, *Macromolecules*, 2024, **57**, 1509–1520.

60 Z. Tong, Y. Xie, M. C. Arno, Y. Zhang, I. Manners, R. K. O'Reilly and A. P. Dove, Uniform segmented platelet micelles with compositionally distinct and selectively degradable cores, *Nat. Chem.*, 2023, **15**, 824–831.

61 P. Schmode, A. Savva, R. Kahl, D. Ohayon, F. Meichsner, O. Dolynchuk, T. Thurn-Albrecht, S. Inal and M. Thelakkat, The Key Role of Side Chain Linkage in Structure Formation and Mixed Conduction of Ethylene Glycol Substituted Polythiophenes, *ACS Appl. Mater. Interfaces*, 2020, **12**, 13029–13039.

62 E. Lee, B. Hammer, J.-K. Kim, Z. Page, T. Emrick and R. C. Hayward, Hierarchical Helical Assembly of Conjugated Poly(3-hexylthiophene)-block-poly(3-triethylene glycol thiophene) Diblock Copolymers, *J. Am. Chem. Soc.*, 2011, **133**, 10390–10393.

63 T. G. Brevé, M. Filius, C. Araman, M. P. van der Helm, P.-L. Hagedoorn, C. Joo, S. I. van Kasteren and R. Eelkema, Conditional Copper-Catalyzed Azide–Alkyne Cycloaddition by Catalyst Encapsulation, *Angew. Chem., Int. Ed.*, 2020, **59**, 9340–9344.

64 J. K. Politis and J. C. Nemes, Synthesis and Characterization of Regiorandom and Regioregular Poly(3-octylfuran), *J. Am. Chem. Soc.*, 2001, **123**, 2537–2547.

65 X.-H. Jin, D. Sheberla, L. J. W. Shimon and M. Bendikov, Highly Coplanar Very Long Oligo(alkylfuran)s: A Conjugated System with Specific Head-To-Head Defect, *J. Am. Chem. Soc.*, 2014, **136**, 2592–2601.

66 J. Qian, X. Li, D. J. Lunn, J. Gwyther, Z. M. Hudson, E. Kynaston, P. A. Rupar, M. A. Winnik and I. Manners, Uniform, High Aspect Ratio Fiber-like Micelles and Block Co-micelles with a Crystalline π-Conjugated Polythiophene Core by Self-Seeding, *J. Am. Chem. Soc.*, 2014, **136**, 4121–4124.

67 H. Cao and P. A. Rupar, Recent Advances in Conjugated Furans, *Chem.–Eur. J.*, 2017, **23**, 14670–14675.

68 B. X. Dong, C. Nowak, J. W. Onorato, T. Ma, J. Niklas, O. G. Poluektov, G. Grocke, M. F. DiTusa, F. A. Escobedo, C. K. Luscombe, P. F. Nealey and S. N. Patel, Complex Relationship between Side-Chain Polarity, Conductivity, and Thermal Stability in Molecularly Doped Conjugated Polymers, *Chem. Mater.*, 2021, **33**, 741–753.

69 M. Watanabe, K. Tsuchiya, T. Shinnai and M. Kijima, Liquid Crystalline Polythiophene Bearing Phenylnaphthalene Side-Chain, *Macromolecules*, 2012, **45**, 1825–1832.